Eur. J. Mineral.
2000, **12**, 835-846

Lead-antimony sulfosalts from Tuscany (Italy): II - Crystal structure of scainiite, $Pb_{14}Sb_{30}S_{54}O_5$, an expanded monoclinic derivative of $Ba_{12}Bi_{24}S_{48}$ hexagonal sub-type (zinkenite group)

YVES MOËLO[1,*], ALAIN MEERSCHAUT[1], PAOLO ORLANDI[2] and PIERRE PALVADEAU[1]

[1] Institut des Matériaux Jean Rouxel - Laboratoire de Chimie des Solides, UMR CNRS 6502, 2, rue de la Houssinière, 44322 Nantes Cedex 3, France

[2] Dipartimento di Scienze della Terra, Università di Pisa, Via S. Maria 53, I-56126 Pisa, Italy

Abstract: The crystal structure of scainiite, $Pb_{14}Sb_{30}S_{54}O_5$, has been solved from single-crystal X-ray data and refined to an *R* index of 8.9 % based on 3703 unique reflections. The structure is monoclinic *C2/m*, with cell parameters *a* 51.996(8), *b* 8.148(1), *c* 24.311(4) Å, β 104.09(1)°, *V* 9990(10) Å^3, and with $Z = 4$. The structure analysis was essential in determining the position of oxygen atoms in a special double-ribbon, $Sb_8(Pb,Sb)_2S_{10}O_5$, directly related to the structure of kermesite, Sb_2S_2O. The general organization of the structure can be described according to the general principles developed by Makovicky (1993) for complex sulfides related to the PbS and SnS archetypes. This structure falls into the group of "pure rod structures" (zinkenite group), and is an expanded homologue of cyclic hexagonal $Ba_{12}Bi_{24}S_{48}$. The expansion of the parent structure is obtained by shearing along a zig-zag surface, that creates lozenge shaped spaces in place of the original hexagonal channels, and filling these spaces by the kermesite-type fragments.

Key-words: scainiite, crystal structure, oxysulfide, lead-antimony sulfosalt, zinkenite group.

Introduction

Numerous studies have been performed among the pure Pb-Sb-S system, and many natural or synthetic solid phases are well known, including their crystal structure. Nevertheless, the addition of a fourth chemical element as a minor component may stabilize an entirely new phase; the best example is that of the mineral dadsonite, where only ~ 0.4 wt. % of chlorine, that is one chlorine atom for about sixty S atoms, is sufficient for its formation (Moëlo, 1979; Makovicky, 1993). The present study relates to the crystal structure of a recently discovered lead-antimony sulfosalt, scainiite (Orlandi *et al.*, 1999), where oxygen also plays a specific crystal chemical role. This crystal structure is topologically an expanded derivative of the hexagonal structure of synthetic $Ba_{12}Bi_{24}S_{48}$, belonging to the zinkenite group (Makovicky, 1985).

1. Crystal structure: general data

The studied crystal is the half part of a needle-like single crystal; the second part was used for the

*e-mail: moelo@cnrs-imn.fr

0935-1221/2000/0012-0835 $ 3.00

Table 1. Atomic coordinates and equivalent/isotropic displacement parameters U(eq/iso) in the crystal structure of scainiite.

Atom	x	y	z	U(eq/iso) (x 10^3)	Atom	x	y	z	U(eq/iso) (x 10^3)
Pb,Sb 1	0.0865(1)	0	0.5547(2)	47(2)	S4	0.2701(5)	½	0.5830(9)	34(7)
Pb,Sb 2	0.0889(1)	½	0.5547(2)	37(1)	S5	0.1899(4)	0	0.9001(9)	27(6)
Pb,Sb 3	0.1450(1)	0	0.4616(2)	31(1)	S6	0.1930(5)	½	0.9032(9)	32(6)
Pb,Sb 4	0.1469(1)	½	0.4659(2)	30(2)	S7	0.4809(4)	0	0.6180(8)	13(5)
Pb5	0.1044(1)	0	0.7367(1)	30(1)	S8	0.4828(5)	½	0.6206(10)	36(7)
Sb5	0.1032(1)	½	0.7553(2)	28(2)	S9	0.1930(4)	0	0.5360(8)	19(6)
Sb6	0.5281(1)	0	0.8069(2)	18(2)	S10	0.1928(5)	½	0.5378(10)	37(7)
Pb6	0.5363(1)	½	0.8044(1)	27(1)	S11	0.2268(4)	0	0.6973(8)	20(6)
Pb7	0.3592(1)	0	0.8647(2)	33(1)	S12	0.2248(4)	½	0.6990(9)	29(6)
Pb8	0.3586(1)	½	0.8694(1)	28(1)	S13	0.1124(4)	0	0.8630(8)	17(5)
Pb9	0.3201(1)	0	0.6790(1)	29(1)	S14	0.1113(5)	½	0.8614(10)	39(7)
Pb10	0.3177(1)	½	0.6780(1)	28(1)	S15	0.5340(4)	0	0.5438(9)	25(6)
Pb11	0.2717(1)	0	0.8101(2)	30(1)	S16	0.5357(4)	½	0.5499(9)	26(6)
Pb12	0.2701(1)	½	0.8049(2)	34(1)	S17	0.2720(5)	0	0.9380(10)	38(7)
Pb13	0.4141(1)	0	0.0298(1)	23(1)	S18	0.2685(4)	½	0.9387(9)	27(6)
Pb14	0.4120(1)	½	0.0279(1)	30(1)	S19	0.3788(5)	0	0.6708(10)	40(7)
Pb15	0.1874(1)	0	0.7808(2)	31(1)	S20	0.3794(4)	½	0.6734(9)	25(6)
Pb16	0.1878(1)	½	0.7805(1)	27(1)	S21	0.3476(4)	0	0.9863(9)	22(6)
Sb7	0.1478(1)	0.2335(6)	0.8861(2)	41(2)	S22	0.3512(4)	½	0.9863(9)	26(6)
Sb8	0.2331(1)	0.2626(6)	0.9228(2)	43(2)	S23	0.4139(5)	0	0.8305(10)	36(7)
Sb9	0.3152(1)	0.2401(6)	0.9656(2)	41(2)	S24	0.4143(5)	½	0.8309(9)	31(6)
Sb10	0.2437(1)	0.2428(6)	0.6479(2)	45(2)	S25	0.5080(5)	0	0.1397(9)	30(6)
Sb11	0.2851(1)	0.2583(7)	0.5217(2)	53(2)	S26	0.5060(4)	½	0.1361(9)	22(6)
Sb12	0.3283(1)	0.2428(6)	0.3801(2)	30(1)	S27	0.4585(5)	0	0.9827(9)	35(7)
Sb13	0.3916(1)	0.2556(5)	0.7405(2)	29(1)	S28	0.4609(5)	½	0.9865(9)	34(7)
Sb14	0.4361(1)	0.2427(6)	0.8998(2)	39(2)	S29	0.3275(3)	0.2495(19)	0.5915(7)	24(4)
Sb15	0.4863(1)	0.2617(6)	0.0644(2)	38(2)	S30	0.3143(3)	0.2505(20)	0.8657(7)	25(5)
Sb16	0.4598(1)	0.2517(5)	0.7580(2)	25(1)	S31	0.3506(3)	0.2524(19)	0.7686(6)	20(4)
Sb17	0.4349(1)	0	0.6379(2)	20(2)	S32	0.4472(3)	0.2479(19)	0.1020(6)	20(4)
Sb18	0.4385(1)	½	0.6402(2)	23(2)	S33	0.2315(3)	0.2479(19)	0.8227(7)	25(4)
Sb19	0.4759(1)	0.2375(7)	0.5412(2)	50(2)	S34	0.2848(3)	0.2477(19)	0.7201(6)	20(4)
Sb20	0.4554(1)	0.2799(6)	0.3482(2)	29(1)	S35	0.3971(3)	0.2522(20)	0.9397(7)	24(4)
O1	0.4487(12)	0	0.7224(24)	45(18)	S36	0.1337(3)	0.2512(20)	0.5328(7)	29(5)
O2	0.4557(8)	½	0.7311(17)	3(12)	S37	0.0887(3)	0.2452(20)	0.6347(7)	28(5)
O3	0.4500(8)	½	0.3133(17)	5(12)	S38	0.0713(3)	0.2431(19)	0.4687(7)	23(4)
O4	0.4422(9)	0.2560(53)	0.6719(19)	47(14)	S39	0.3515(3)	0.2527(20)	0.2142(7)	24(4)
S1	0.1483(4)	0	0.6591(9)	25(6)	S40	0.4308(3)	0.2158(21)	0.2427(6)	23(4)
S2	0.1492(5)	½	0.6594(10)	36(7)	S41	0.4957(3)	0.2319(19)	0.2575(6)	21(4)
S3	0.2664(4)	0	0.5838(9)	28(6)					

Mixed-site occupancy: (Pb,Sb)1 and (Pb,Sb)4, 1/3 Pb + 2/3 Sb; (Pb,Sb)2 and (Pb,Sb)3, 2/3 Pb + 1/3 Sb. Unit-cell parameters (space group $C2/m$): a = 51.996(8) Å, b = 8.148(1) Å, c = 24.311(4) Å, β = 104.09(1)°, V = 9990(10) Å^3.

electron probe micro-analysis, and gave the composition (wt. %): Pb 36.99(33), Sb 41.80(37), S 20.39(20), O 0.65(15), Total 99.83(64) (Orlandi *et al.*, 1999). The size of the crystal fragment used for X-ray study is close to a parallelepiped with dimensions 0.05 x 0.10 x 0.32 mm^3; it was mounted on a STOE IPDS single φ axis diffractometer with a 2D area detector based on Imaging Plate technology. The diffraction pattern was stored as latent image on the image plate, after an exposure time of 3 mn for each φ-position. 260 images were recorded at ambient temperature (293 K) by using the rotation method 0° < φ < 260° at intervals of 1°. Because of large unit-cell parameters, the crystal-to-detector distance was set to 120 mm, that could satisfy, *a priori*, a good reflection resolution. A total of *ca* 31 h was required for the data collection. The images were processed with the set of programs from STOE (DISPLAY, INDEX, CELL, PROFILE, INTEGRATE) (Stoe, 1996). Using the Mo $K\alpha$ radiation (λ = 0.71073 Å, 50 kV x 40 mA), 29131 reflections (14546 to be merged and 14585 systematically absent) were measured to a maximum 2θ of 36.54°, among which 3750 were unique after merging; this corresponds to 94.8 % completion at this 2θ limit (merging R value = 0.0877). This data set was employed for structure solution attempts. The lattice parameters determined by the image plate system were: a = 51.996(8) Å, b = 8.148(1) Å, c = 24.311(4) Å and β = 104.087(13)°.

The structure of scainiite was partly solved by

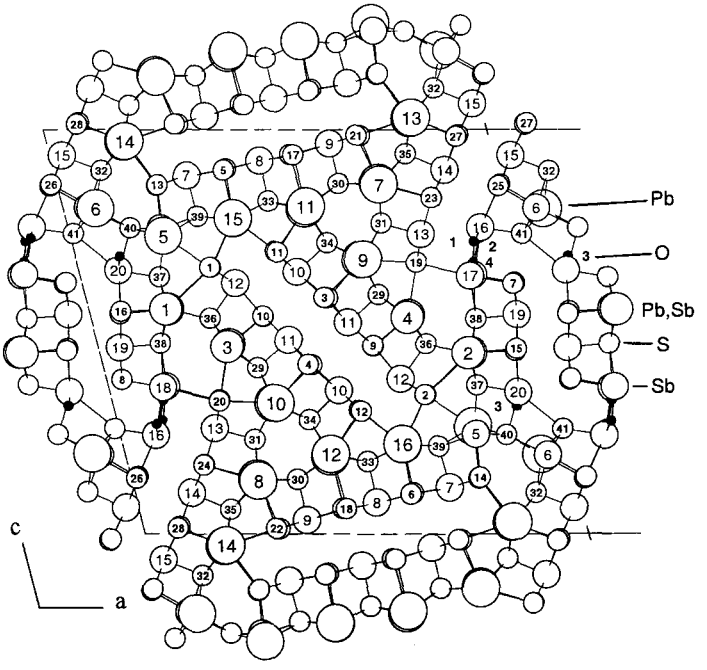

Fig. 1. Projection of the scainiite crystal structure along **b** (half-unit-cell c x $a/2$), with atom labelling according to Table 1. Increasing atom size: O (full circle), S, Sb, (Pb, Sb) and Pb (empty circles). Labelled atoms have $y = 0$ (position *4i*), or ~1/4 (position *8j*).

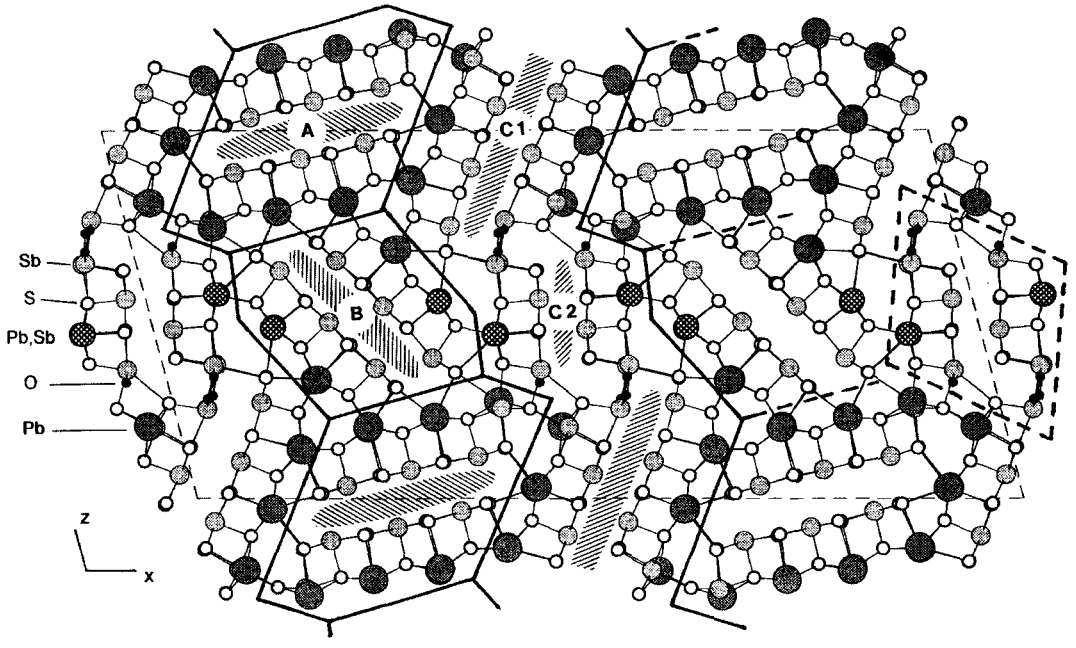

Fig. 2. Organization of the scainiite crystal structure around lone-electron-pair micelles (projection along **b**). Increasing atom size: O (full circle), S (empty circle), Sb (light grey), (Pb, Sb) (crossed hatched) and Pb (medium grey). Thick lines (left part): rods A and B. C1 and C2: long and short SnS-type interfaces in the C central layer. Lozenge at the right side (dashed lines): kermesite-type rod. Dashed areas: lone-electron-pair micelles.

means of direct methods, and the final solution was found from subsequent difference-Fourier syntheses. Refinement was conducted in the space group *C*2/*m* (n° 12) on data corrected for absorption effects with the faces-indexed option of the SHELXTL program (Sheldrick, 1996) (crystal idealized with size ~ 0.05 x 0.10 x 0.32 mm^3, bounded by faces {100}, {001} and {010}; μ = 33.30 mm^{-1}; minimum and maximum transmission factors: 0.0234 and 0.1783).

For intermediate refinements, we also considered bond lengths and bond valence calculations (Brese & O'Keeffe, 1991) to assign the most probable Pb/Sb atomic ratios of mixed (Pb, Sb) sites, where the refined atomic coordinates as well as the displacement parameters are constrained to be identical whatever the cation (Table 1). We were also aware of the charge equilibrium taking into account the formal oxidation states of +II (Pb), +III (Sb), -II (S and O). However, because of too large uncertainties on the results of these calculations, occupancies for these mixed (Pb, Sb) sites were adjusted at the simplified ratios 1/3-2/3 or 2/3-1/3, which respect the homogeneity of displacement parameters. It would have not been reasonable to refine the relative percentages between Pb and Sb, even with the constraint that the sum of occupancies is 100 %, because the condition to get an exact charge balance is not so easy to introduce.

The final refinement converged to a reliability factor R_1 = 0.0891 for 3703 unique reflections (R_1 = 0.0824 for 3020 reflections with $F_o > 4\ \sigma(F_o)$) with 379 variables. Such a high value of R_1 is mainly due to the bad quality of the crystal. All Pb and Sb atoms were refined anisotropically. The final electron density map with coefficients F_o-F_c shows maximum and minimum at 2.69 and -3.74 $e^-.Å^{-3}$, respectively. The highest residuals are found within 1 Å around Pb atoms. Atomic coordinates and displacement parameters (U_{eq} and U_{iso}) are reported in Table 1.

The general structural scheme projected parallel to **b** is given on Fig. 1 (half-unit-cell *c* x *a*/2) and Fig. 2. The unit cell contains 77 independent positions, 32 corresponding to cations, 45 to anions (Table 1). Among cation positions 12 are pure Pb, 16 pure Sb, and 4 mixed (Pb, Sb). Among anion positions, 41 are filled by S, and 4 by O. Oxygen atoms are located in a specific fragment of the structure (dashed lozenge of Fig. 2, enlarged in Fig. 3a). Taking into account the multiplicity of each site (with 100 % occupancy in all of them and no additional cation), and respecting valence balance with Pb^{2+}, Sb^{3+}, S^{2-} and O^{2-}, the ideal structural formula is $Pb_{14}Sb_{30}S_{54}O_5$, with Z = 4. The unit cell contains 412 atoms, with V = 9990 $Å^3$, and the calculated density is 5.56.

Table 2 indicates bond lengths and coordina-

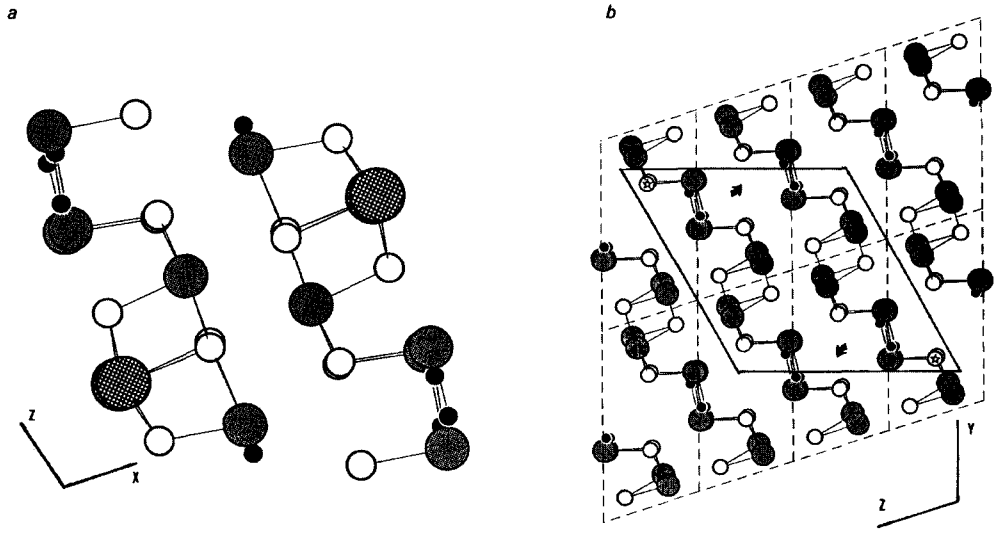

Fig. 3. a: projection along **b** of the kermesite-type rod (double ribbon) of the structure of scainiite (dashed lozenge of Fig. 2). b: Projection of the kermesite structure along **a** (2*b* x 4*c* cell). Layers parallel to (011) are clearly visible. Central lozenge (solid line): double ribbon parallel to **a**, with formula $(Sb_{10}S_{10}O_6)_\infty$. The two arrows indicate the final position of sulfur atoms (white star) after a half-turn rotation around Sb.

Table 2. Interatomic distances (Å) around cations, with corresponding bond valences (b.v.) calculated according to Brese & O'Keeffe (1991).

Metal-Anion	Length	b.v.	Metal-An.	Length	b.v.	Metal-An.	Length	b.v.	Metal-An.	Length	b.v.
(Pb,Sb)1-S16	2.62(2)	0.70	Pb8 -S22	2.96(2)	0.33	Pb16 -S39	2.93(2)	0.36 x2	Sb14 -S35	2.46(2)	0.97
-S37	2.77(2)	0.46 x2	-S30	3.05(2)	0.26 x2	-S6	2.93(2)	0.36	-S23	2.67(2)	0.55
-S38	2.85(2)	0.37 x2	-S35	3.06(2)	0.25 x2	-S33	3.05(2)	0.26 x2	-S24	2.75(2)	0.44
-S36	3.34(2)	0.10 x2	-S31	3.12(2)	0.21 x2	-S12	3.08(2)	0.24	-S27	2.86(2)	0.33
	Sum =	**2.56**	-S24	3.26(2)	0.15	-S2	3.13(2)	0.21	-S28	3.03(2)	0.21
(Pb,Sb)2-S15	2.80(2)	0.47		Sum =	**1.92**		Sum =	**2.05**		Sum =	**2.50**
-S37	2.85(2)	0.41 x2	Pb9 -S29	3.03(2)	0.27 x2	Sb7 -S39	2.45(2)	1.00	Sb15 -S32	2.43(2)	1.06
-S38	2.94(2)	0.32 x2	-S34	3.06(2)	0.25 x2	-S13	2.61(2)	0.65	-S26	2.64(2)	0.60
-S36	3.23(2)	0.15 x2	-S19	3.11(3)	0.22	-S14	2.85(2)	0.34	-S28	2.81(2)	0.38
	Sum =	**2.23**	-S31	3.13(3)	0.21 x2	-S5	2.86(2)	0.33	-S25	2.86(2)	0.33
(Pb,Sb)3-S9	2.70(2)	0.62	-S3	3.16(3)	0.19	-S6	3.16(2)	0.15	-S27	3.03(2)	0.21
-S36	2.83(2)	0.43 x2		Sum =	**1.87**		Sum =	**2.47**		Sum =	**2.58**
-S29	2.96(2)	0.30 x2	Pb10 -S4	2.94(2)	0.35	Sb8 -S33	2.42(2)	1.08	Sb16 -O4	2.07(4)	0.77
-S29	3.22(2)	0.15	-S34	3.01(2)	0.29 x2	-S18	2.63(2)	0.61	-O2	2.12(1)	0.67
	Sum =	**2.23**	-S29	3.06(2)	0.25 x2	-S6	2.80(2)	0.39	-O1	2.25(2)	0.47
(Pb,Sb)4-S10	2.59(3)	0.75	-S31	3.16(2)	0.19 x2	-S17	2.90(2)	0.30	-S41	2.44(2)	1.03
-S36	2.79(2)	0.44 x2	-S20	3.24(2)	0.15	-S5	3.05(2)	0.20		Sum =	**2.94**
-S29	2.96(2)	0.28 x2		Sum =	**1.96**		Sum =	**2.58**	Sb17 -O1	2.00(6)	0.93
-S19	3.26(2)	0.12	Pb11 -S33	2.98(2)	0.31 x2	Sb9 -S30	2.42(2)	1.08	-O4	2.24(4)	0.49 x2
	Sum =	**2.31**	-S30	3.07(2)	0.25 x2	-S21	2.55(2)	0.76	-S7	2.55(2)	0.76
Pb5 -O3	2.80(2)	0.16	-S17	3.11(2)	0.22	-S22	2.79(2)	0.40	-S19	3.21(2)	0.13
-S13	3.00(2)	0.30	-S11	3.14(2)	0.20	-S17	2.93(2)	0.27	-S38	3.29(2)	0.10 x2
-S39	3.06(2)	0.25 x2	-S34	3.17(2)	0.19 x2	-S18	3.17(2)	0.14		Sum =	**3.00**
-S40	3.07(2)	0.25 x2		Sum =	**1.92**		Sum =	**2.65**	Sb18 -O4	2.12(4)	0.67 x2
-S37	3.13(2)	0.21 x2	Pb12 -S33	2.97(2)	0.32 x2	Sb10 -S34	2.41(2)	1.11	-O2	2.17(4)	0.59
-S1	3.29(2)	0.14	-S12	3.04(2)	0.27	-S11	2.58(2)	0.71	-S8	2.46(2)	0.97
	Sum =	**2.02**	-S34	3.14(2)	0.20	-S12	2.74(2)	0.46	-S38	3.25(2)	0.12 x2
Sb5 -S40	2.50(2)	0.87 x2	-S30	3.16(2)	0.19 x2	-S3	2.94(2)	0.27		Sum =	**3.14**
-S14	2.51(2)	0.85	-S18	3.27(2)	0.14	-S4	3.14(2)	0.15	Sb19 -S38	2.41(2)	1.11
-S39	3.08(2)	0.18 x2		Sum =	**1.83**		Sum =	**2.70**	-S7	2.66(2)	0.57
	Sum =	**2.95**	Pb13 -S27	2.82(2)	0.48	Sb11 -S29	2.43(2)	1.06	-S15	2.79(2)	0.40
Pb6 -S26	2.91(2)	0.38	-S32	2.94(2)	0.35 x2	-S4	2.70(2)	0.51	-S8	2.84(2)	0.35
-S41	2.93(2)	0.36 x2	-S35	2.98(2)	0.31 x2	-S9	2.81(2)	0.38	-S16	3.03(2)	0.21
-S32	3.03(2)	0.27 x2	-S14	3.23(2)	0.16	-S3	2.90(2)	0.27		Sum =	**2.64**
-S40	3.25(2)	0.15 x2	-S21	3.26(2)	0.11	-S10	2.94(2)	0.27	Sb20 -O3	1.98(2)	0.98
	Sum =	**1.94**		Sum =	**2.07**		Sum =	**2.52**	-S37	2.44(2)	1.03
Sb6 -S25	2.53(2)	0.81	Pb14 -S35	2.91(2)	0.38 x2	Sb12 -S36	2.52(2)	0.83	-S40	2.63(2)	0.61
-S41	2.57(2)	0.72 x2	-S28	2.95(2)	0.34	-S2	2.60(2)	0.67	-S16	3.03(2)	0.23
-S32	3.04(2)	0.20 x2	-S32	3.03(2)	0.27 x2	-S1	2.71(2)	0.49		Sum =	**2.85**
-S40	3.22(2)	0.12 x2	-S22	3.08(2)	0.24	-S10	3.19(2)	0.14			
	Sum =	**2.89**	-S13	3.21(2)	0.17	-S9	3.30(2)	0.10			
Pb7 -S31	3.06(2)	0.25 x2		Sum =	**2.05**		Sum =	**2.22**			
-S30	3.11(2)	0.22 x2	Pb15 -S5	2.87(2)	0.42	Sb13 -S31	2.39(2)	1.18			
-S35	3.11(2)	0.22 x2	-S39	2.88(2)	0.41 x2	-S20	2.55(2)	0.75			
-S23	3.15(2)	0.20	-S33	3.04(2)	0.27 x2	-S19	2.67(2)	0.55			
-S21	3.16(2)	0.20	-S1	3.16(2)	0.19	-S24	2.99(2)	0.23			
	Sum =	**1.77**	-S11	3.22	0.16	-S23	3.04(2)	0.20			
				Sum =	**2.13**		Sum =	**2.91**			

tions around cations, with bond valences calculated according to Brese & O'Keeffe (1991). It permits to discriminate on one hand well defined atomic positions, with a bond valence sum (Σbv) close to the expected one of the selected atom, and, on the other hand, atomic positions with a significant deficit of Σbv, that corresponds probably to mean positions, and may partly contribute to the high value of R (~ 0.09). Additional comments are given in the detailed description of the structure.

2. Modular analysis of the structure

According to the general principles of modular analysis developed by Makovicky (1993), the scainiite structure can be described through various ways, presented hereafter.

2.1 – Organization around lone-electron-pair micelles

One of the main topological features of the

crystal structures of Pb-Sb sulfosalts is the ordering of Sb atoms to form lone-electron-pair micelles (Makovicky & Mumme, 1983). Taking into account such lone-electron-pair micelles, Fig. 2 (left part) shows two classic rods A and B, forming layers parallel to (100), and alternating along **a** with a complex layer C ("ribbon-layer"). The rods A and B are directly derived from the SnS archetype (Makovicky, 1985), elongated along $(001)_{SnS}$, four-atom thick (that is one unit a_{SnS}), and three b_{SnS} large (= 3 Q). Fringing cations are Pb, (Pb, Sb), or Pb and Sb alternatively, while inner ones are purely Sb, constituting the lone-electron-pair micelles. In these micelles, each Sb electron pair is pointing between two S atoms, and *vice versa*. The unit formula of rod A is 2 x $(Me_{12}S_{16})$, exactly $Pb_{10}Sb_{14}S_{32}$, that of rod B, 2 x $(Me_{10}S_{14})$, exactly $Pb_6Sb_{14}S_{28}$.

The C layer is composed of complex ribbons, two-atom thick, containing a kermesite-type fragment (Fig. 2 and 3a - see 2.2). In this fragment, the Sb_2O_2 ladder (Fig. 4b) induces an inversion of the SnS-type interface ("antiphase boundary"), and two consecutive ribbons show alternatively a long (4Q) and a short (2Q) interface (elongation parallel to $(001)_{SnS}$), with corresponding long and short lone-electron-pair micelles (C1 and C2). Oxygen atoms omitted, the long interface shows perpendicularly to $(001)_{SnS}$ the sequence defect S-Sb-Sb-S, corresponding in the short interface to the sequence Sb-S-S-Sb. A similar inversion has been described in various synthetic compounds with incommensurate sandwiched layered structure, $(BiSe)_{1.10}TaSe_2$ (Zhou *et al.*, 1992; Petricek *et al.*, 1993), $(BiS)_{1.11}NbS_2$ (Gotoh *et al.*, 1995), $(SbS)_{1.15}TiS_2$ and $(SbS)_{1.15}(TiS_2)_2$ (Ren *et al.*, 1995, 1996), where in the pseudo-tetragonal, diatomic-thick layer (Q type), the inversion is due to $(Bi_2)^{4+}$ or $(Sb_2)^{4+}$ pairs. In pääkkönenite, Sb_2AsS_2 (Bonazzi *et al.* , 1995), where As acts as an anion, one observes the sequence Sb-S-Sb-As-S..., due to the formation of $(As_2)^{-4}$ pairs, that permits the layered organization of the structure (contrary to the rod structure of the parent compound stibnite, Sb_2S_3).

Without oxygen, the simplified formula of the C ribbon is 2 x $(Me_{11}S_{12})$. With oxygen atoms and distribution of Pb and Sb, it gives $Pb_6Sb_{16}S_{24}O_5\square$ ($\square$ = oxygen vacancy – see Fig. 4b). Thus the whole structural formula of scainiite corresponds to A + B + 2 C: $Pb_{10}Sb_{14}S_{32}$ + $Pb_6Sb_{14}S_{28}$ + 2 $Pb_6Sb_{16}S_{24}O_5\square$ = 2 $Pb_{14}Sb_{30}S_{54}O_5\square$.

All Sb atoms forming the lone-electron-pair micelles A, B and C1 have hemi-octahedral (= square pyramidal) coordination with S, with generally a low bond valence sum (Σbv from 2.22 up to 2.91 v.u. (valence unity) - mean 2.57 v.u.). Nevertheless, the apical bond always corresponds to a strong bond of about 1 v.u. (Σbv from 0.82 up to 1.18 v.u.). Thus the bond valence deficit could be due to an imprecision in the relative position between the Sb atom and the four S atoms of the pyramid basis. This deficit may indicate that the coordinates of Sb and surrounding four S are mean positions. The complexity of the structure, increased by the poor quality of the studied crystal did not permit the search for a multi-site model.

Among these Sb atoms, Σbv of Sb12 is particularly low (2.22 v.u.), and difficult to explain.

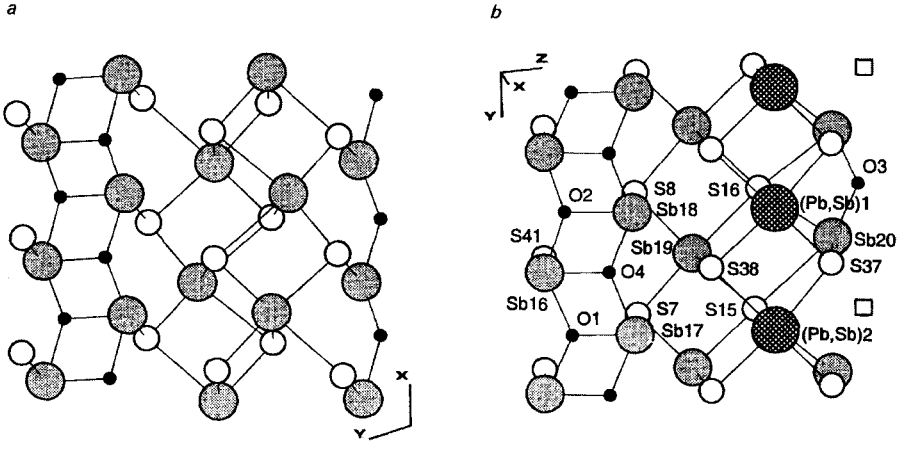

Fig. 4. a: Projection along **c** of the kermesite fragment selected in Fig. 3b, showing the Sb_2O_2 ladder on one side, and Sb-O chain (half of the ladder) on the other side. b: similar projection (slightly oblique to **a**) of one of the two kermesite-type ribbons of scainiite selected in Fig. 3a. One recognizes the same Sb_2O_2 ladder, but on the other side half of the O atoms of the Sb-O chain are lacking (the two squares represent these oxygen vacancies).

One explanation would be a mixed (Pb,Sb) site, but this would need a Pb/Sb atomic ratio close to 1 for a good adequation between mean valence (2.50) and newly calculated one (2.55), with too high a value of U_{iso}.

2.2 – Weak-bond surface cut-out: the $(20\bar{1})$ rod-layer

The scainiite structure may also be described as rod-layers parallel to $(20\bar{1})$, if the structure is cut out along the zig-zag surfaces passing through the lone-electron-pair micelles (that is the surfaces of weakest bonding - Fig. 5; see the example of nuffieldite structure - Moëlo *et al.*, 1997). One of these two zig-zag surfaces (solid line in Fig. 5) shows consecutive segments with a bending angle close to 120°: such a surface may act as a (bad) cleavage plane, and also a glide plane parallel to **b**; it may also correspond to a well developed crystal face. The second surface (dashed line in Fig. 5) shows accute bending angles close to 60°: it would hardly act as a cleavage plane, but may also play the role of a glide plane along **b**. If one selects half of each layer (between solid and dashed lines), one easily recognizes in this sub-layer the regular succession of a pseudo-ternary cyclic rod typical of the zinkenite group (Makovicky, 1985), with an oxy-sulfide ribbon.

Two adjacent cyclic rods have been selected in Fig. 6a. In order to maintain the ternary pseudo-symmetry, they have been completed at two of the three apices by atoms from the kermesite-type ribbons. According to Makovicky (1985, 1993), these cyclic rods of scainiite, with composition $Pb_{12}(Pb, Sb)_4Sb_{20}S_{48}$, are topologically identical with the cyclic unit rods constituting the building blocks of hexagonal $Ba_{12}Bi_{24}S_{48}$ (Aurivillius, 1983 - Fig. 6b; isotypic with $Eu_{13.2}Bi_{24}S_{48}$ - Lemoine *et al.*, 1986).

All Pb atoms are located in these triangular columns. Six Pb atoms (no. 7 to 12) around the pseudo-ternary axis show a bicapped trigonal prismatic coordination, with Σbv between 1.77 and 1.96 v.u. (Table 2). Four other Pb atoms (two pairs, no. 13-14 and 15-16 - Σbv between 2.05 and 2.13 v.u.) are positioned close to the extremities of the lone-electron-pair micelles between trigonal rods, with a monocapped trigonal prismatic coordination. The last two Pb atoms (no. 5 and 6 - Σbv 2.02

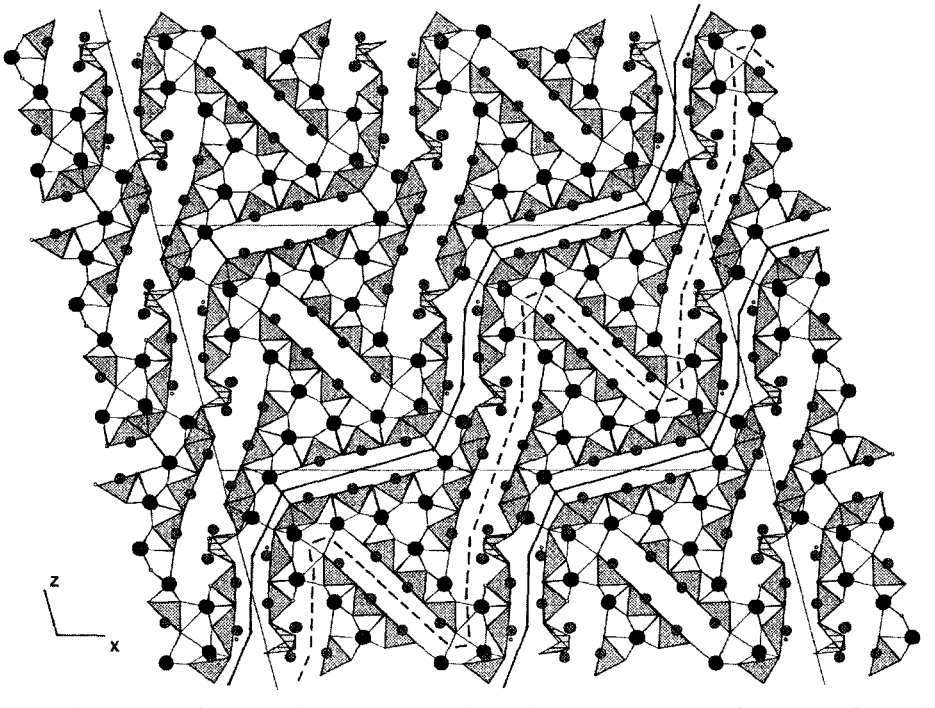

Fig. 5. Extended projection along **b** of the structure of scainiite, indicating two types of zig-zag surfaces of weak bonding. The two solid lines delimitate one $(20\bar{1})$ rod-layer; the central dashed one separates the two constituting sub-layers. Grey triangles represent the sulfur hemi-octahedra around Sb atoms; small hatched triangles connect O and S atoms around the Sb atoms of the "antiphase boundaries".

and 1.94 v.u.) alternate with Sb ones (no. 5 and 6 - Σbv 2.94 and 2.89 v.u.) at two apices of the rod.

The four mixed (Pb, Sb) positions (no. 1 to 4) are located around S36, at the apex connected with the oxy-sulfide ribbon (Fig. 6a). The total occupancy of these four sites corresponds to 2 Pb + 2 Sb, with a Pb/Sb atomic ratio fixed to 1/2 for sites n° 1 and 4, and inversely to 2/1 for sites n° 2 and 3. Σbv is always lower than that expected for the Pb/Sb ratio (Table 2); this shift could likely be due to the choice of a common averaged position for Pb and Sb. Changing the Pb/Sb ratio for a higher Pb content would better fit the Σbv value, but correspondingly would abnormally increase the U_{eq} value.

The oxy-sulfide ribbon is topologically quite identical to a ribbon extracted from the layered structure of kermesite (Kupcik, 1967 – compare Fig. 3a and b). The only difference is a half-turn rotation of the 3-coordinated Sb atom at the margin of the selected ribbon (arrows in Fig. 3b). One must point out that the selected part of the kermesite layer is larger than the unit ribbon $Sb_4S_4O_2$, and corresponds to a double $Sb_5S_5O_3$ fragment (in scainiite, $Sb_8(Pb,Sb)_2S_{10}O_5\square$). The projection, perpendicular to the elongation, of these two ribbons (Fig. 4a: kermesite; Fig. 4b: scainiite) shows that in scainiite the oxygen position O3 has no pseudo-symmetrical equivalent with a *b*/2 translation (vacancy □ of the formula above), which explains the true ~ 8 Å periodicity along **b**, with the *b*/2 substructure (and the ordered alternation along **b** of the two pairs Pb5 + Sb5, on the one hand, and Pb6 + Sb6, on the other hand, close to this oxygen atom). This vacancy also explains the *a*/2 substructure.

The coordination of oxygen in the oxy-sulfide ribbon of scainiite is thus directly derived from its bonding in the structure of kermesite, where two oxygen atoms (in triangular coordination) form with two Sb atoms a (Sb-O) ladder parallel to **b** (Fig. 4a). But in scainiite the four oxygen atoms have distinct bondings with Sb atoms (Fig. 4b), as reported in Table 3 (bond distances and valences; angles). O1, O2 and O4 have a planar triangular coordination; O2 is the most symmetrical, when O1 has a strong bond with Sb17, and O4 an intermediate bonding scheme. O3 is bound only to two Sb atoms, with an angle close to 131°. Nevertheless, one must point out the short distance between O3 and Pb5 (2.80 Å), that may indicate a weak bonding (bond valence of 0.16 v.u.). Σbv is quite good for all these four oxygen atoms (1.87 to 1.96 v.u. - Table 3).

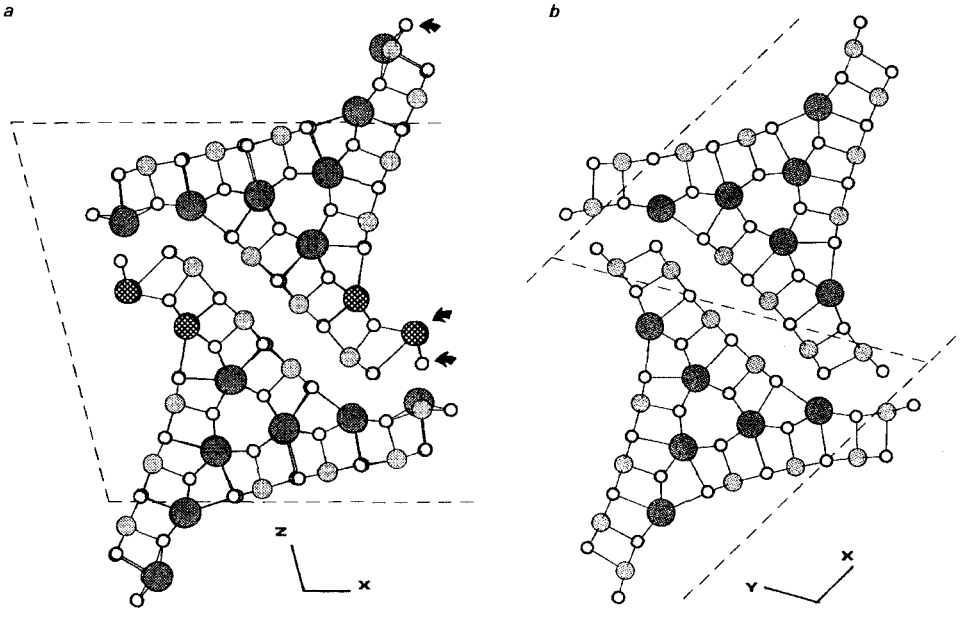

Fig. 6. a: Selection of two adjacent pseudo-ternary cyclic rods from a $(20\bar{1})$ rod-layer in the structure of scainiite (atom labelling: see Fig. 1). Arrows at the apices indicate additional atoms from the kermesite-type ribbons. b: Two equivalent cyclic rods from the crystal structure of $Ba_{12}Bi_{24}S_{48}$ (Aurivillius, 1983). In order of decreasing size: Ba (dark grey), Bi (light grey) and S (open cicles). Here there is a *b*/2 shift between these two rods (derivation from the PbS archetype).

Table 3. Oxygen atoms in the structure of scainiite: coordination, bond lengths (Å), bond valences and angles. Σbv: bond valence sum.

Atom	Coord.	Sb atom	Length	Bond val.	Σbv	Angle
O1	3	(16) x 2	2.25	0.47 x 2	1.87	Sb16 -O- Sb16' = 132°
		(17)	2.00	0.93		Sb16 -O- Sb17 = 113° (two)
O2	3	(16) x 2	2.12	0.67 x 2	1.93	Sb16 -O- Sb16' =145°
		(18)	2.17	0.59		Sb16 -O- Sb18 = 107° (two)
O3	2	(20) x 2	1.98	0.98 x 2	1.96*	Sb20 -O- Sb20' = 131°
O4	3	(16)	2.07	0.77	1.93	Sb17 -O- Sb18 = 138°
		(17)	2.24	0.49		Sb17 -O- Sb16 = 111°
		(18)	2.12	0.67		Sb18 -O- Sb16 = 111

*without adding Pb5 at 2.80 Å (0.16 v. u.)

The Sb atoms forming the (Sb-O) ladder (no. 16, 17 and 18 - Fig. 4b) are strongly bound to one S and three O atoms, with only a weak bonding with other S atoms (Σbv from 2.80 to 2.94 v.u.): they can be described as sharing one 5p electron with the S atom, and the two other electrons with the three O atoms. Sb20 has two strong bonds (~ 1 v.u. each) with O3 and S37, with the third valence shared principally among two S (Σbv = 2.85 v.u.); now only one 5p electron is shared with O, and the two others with S atoms. The last Sb atom (n° 19) is bound exclusively with S, with a hemi-octahedral coordination (Σbv = 2.64 v.u.).

Finally, in this rod-layer cut-out, the scainiite structure results from the one-for-one sequence of a $Ba_{12}Bi_{24}S_{48}$-type building block with a kermesite-type ribbon, giving the sub-layer parallel to $(20\bar{1})$:

$$Pb_{12}(Pb, Sb)_2Sb_{20}S_{44}^* + (Pb, Sb)_2Sb_8S_{10}O_5\square = Pb_{12}(Pb, Sb)_4Sb_{28}S_{54}O_5\square$$

(*: after subtraction of the atoms at the apices shared with the kermesite-type ribbon: 2 (Pb, Sb) + 4 S).

As explained for the nuffieldite structure (Moëlo *et al.*, 1997), such a cut-out according to the surfaces of weakest bonding is a way for understanding the possible building process of scainiite structure at the unit-cell level: after formation of 1D building blocks (kermesite-type ribbon and helicoidal rod), bonding of these 1D blocks to form $(20\bar{1})$ rod-layers (1D to 2D polymerization), and finally agglomeration of these layers (2D to 3D polymerization).

2.3 – Derivation from the hexagonal $Ba_{12}Bi_{24}S_{48}$ parent structure

Fig. 7a points again to the pseudo-ternary helicoidal rods, but in a different way. Each rod, with the simplified formula 2 x $(Me_6S_8)_3$, has the effective composition $Pb_{14}Sb_{22}S_{48}$. Six among these rods have been selected around one central, kermesite-type fragment. This fragment, omitted in the middle of the figure, is restricted to a $(Sb_6S_6O_4)_2$ unit (empty rod with lozenge section). These empty rods permit the compression of the structure through a (2Q)-translation (arrows) along the dashed segments. One obtains finally a pseudo-hexagonal structure (Fig. 7b), very close to that of synthetic hexagonal $Ba_{12}Bi_{24}S_{48}$ (Aurivillius, 1983 - Fig. 7c). In Fig. 7b, the first S-atom circular envelope around the pseudo-hexagonal axis has been outlined (hexagon – cut in two halves in Fig. 7a).

The main difference between this hypothetic compressed structure and synthetic $Ba_{12}Bi_{24}S_{48}$ is the replacement of Sb by Bi in the synthetic compound, that gives a PbS-type connection (and not a SnS-type one) between adjacent helicoidal rods, and thus a ~ 2 Å *b*-shift between two adjacent rods (the pseudo-6-fold rotation axis is replaced by a 6_3 axis). In the pseudo-hexagonal axis (Fig. 7b), there remain two Sb_2O groups, too close to be retained together. There are two ways to respect the valence equilibrium: 1 – suppression of these two Sb_2O groups, with the formula $Pb_{12}Sb_{24}S_{48}$ for each rod, and 2 – suppression of only one half of these groups, with conservation of the rod composition $Pb_{14}Sb_{22}S_{48}$, giving the final formula $Pb_{14}Sb_{23}S_{48}O_{0.5}$.

The latter hypothesis points to the problem of the true chemical formula of the two forms of $BaBi_2S_4$ described by Aurivillius (1983). According to this author, these two forms have their structural formula close to $Ba_9Bi_{18}S_{36}$ and $Ba_{12}Bi_{24}S_{48}$, but with a slight Bi_2S_3 excess in the first compound, and a BaS excess in the second one. The BaS excess is explained by a partial Ba occupancy on the hexagonal axis (at *c*/4 and 3*c*/4), together with some Bi vacancies; however, this Ba position gives three too short Ba-S distances at

2.96 Å. The position of the extra atom on the hexagonal axis is certainly a mean of (at less) six eccentric positions, which might better correspond to Bi atoms, together with some (Bi, Ba) mixing on other positions. Such a model has been proposed for the crystal structure of zinkenite (Portheine &

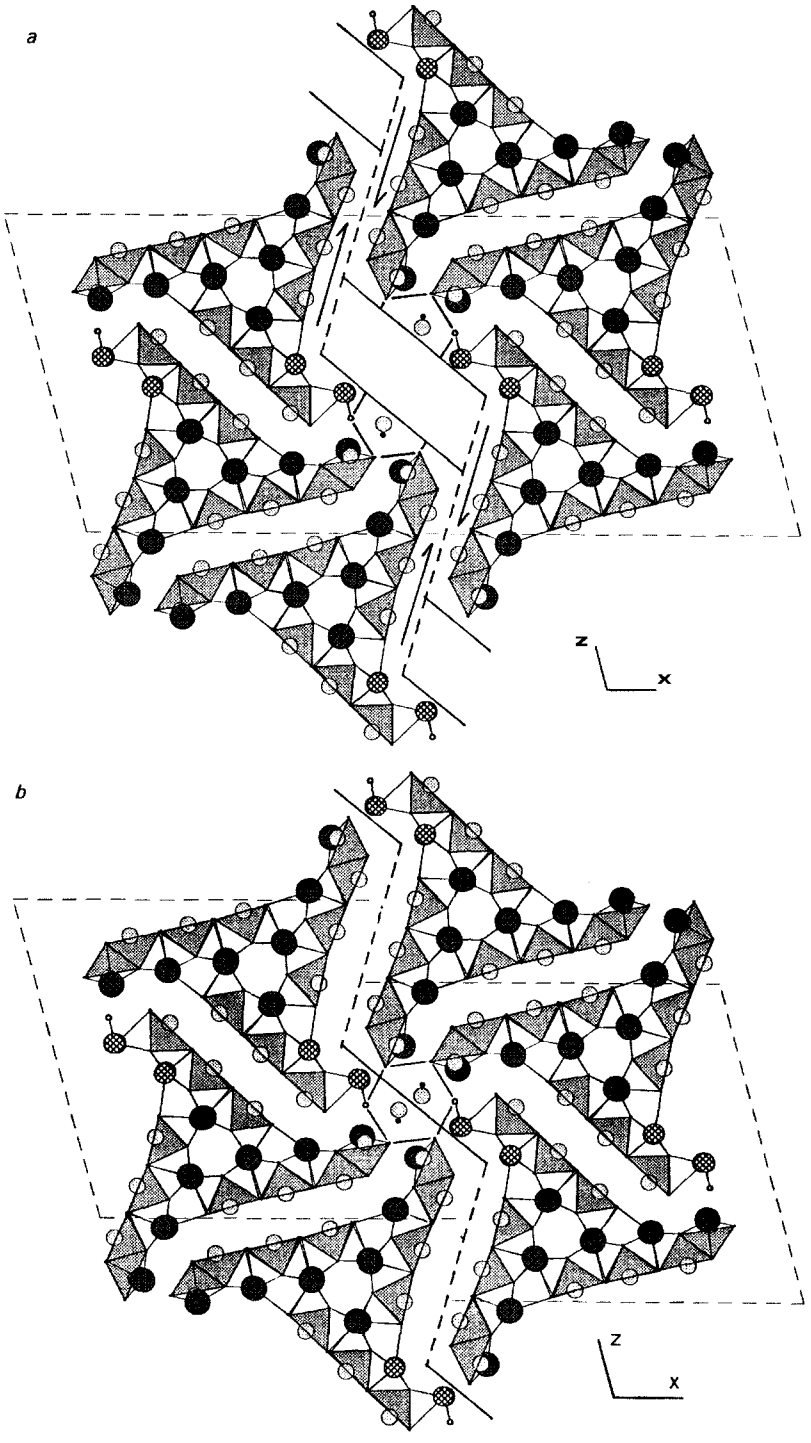

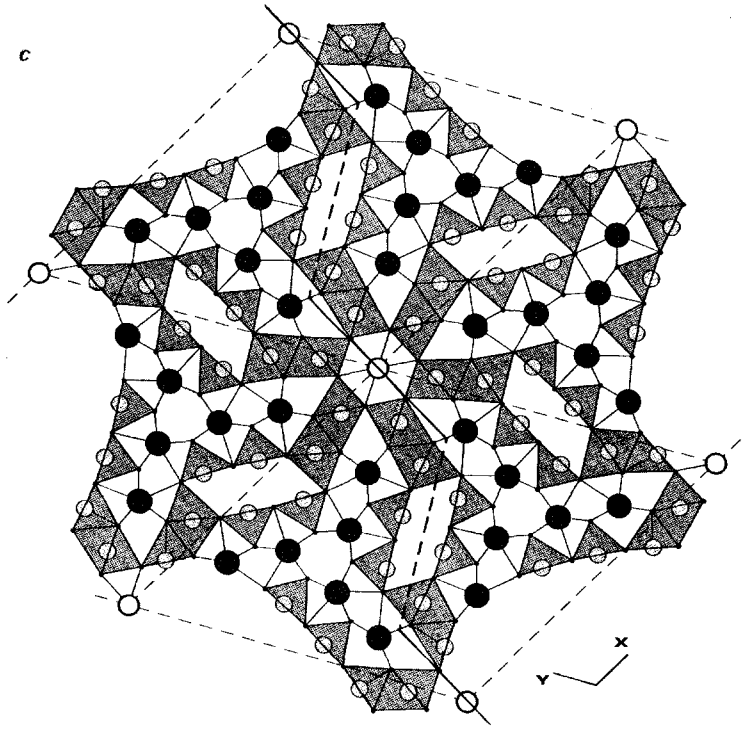

Fig. 7. a: Selection of six pseudo-ternary cyclic rods in scainiite structure, together with suppression of a central, kermesite-type rod (empty lozenge). Dashed lines indicate the gliding surface, and arrows, the 2Q-compression direction. b: Result of the compression. The central hexagon connects the first S-atom circle around the pseudo-hexagonal axis. c: Equivalent projection on the *ab*-plane of six helicoidal rods around one 6_3 axis in the crystal structure of $Ba_{12}Bi_{24}S_{48}$ (Aurivillius, 1983). Small circles: Bi atoms, with octahedral or hemi-octahedral coordination with sulfur (shaded lozenges and triangles); dark circles: Ba; open circles indicate cations on the hexagonal axis. The zig-zag solid/broken line corresponds to the surface of compression of Fig. 7a and b.

Nowacki, 1975). One cannot also exclude some oxygen atoms bonded with Bi atoms in the hexagonal channel, that may stabilize this structure type.

Conclusion

The crystal structure of scainiite is an expanded, monoclinic derivative of hexagonal $Ba_{12}Bi_{24}S_{48}$, after cutting this parent structure in a zig-zag fashion, and gliding the two parts of the structure along one direction (~ [210]) of the zig-zag line (dashed segments of Fig. 7c). It opens an empty rod-like space, with lozenge section, which can be filled by a kermesite-type double-ribbon, that blocks the final structure. One thus obtains a homologous derivative of the accretional type (Makovicky, 1989), but here the expansion module is not a layer, but an "en échelon" rod row. In the general classification of rod-layer sulfosalts (Makovicky, 1993), scainiite belongs, together with kobellite and related sulfosalts, to the subgroup of non-hexagonal derivatives of parent members of the zinkenite group (or group of cyclically twinned rod-based sulfosalt structures).

The crystal structure of scainiite is an original case study for the application of structural modular analysis developed by Makovicky (1993) for complex sulfides related to the PbS archetype. It is a new example illustrating how a supplementary anion in low concentration permits the formation of an original structure through a new connection way of building blocks of the rod type. Another interesting example where oxygen acts as a minor component is described by Sutorik & Kanatzidis (1994), for the synthetic compound $Ba_6Ti_5S_{15}O$: here the oxygen atoms break infinite single chains of face-sharing TiS_6 octahedra present in the $BaTiS_3$ parent structure.

In scainiite, oxygen atoms are bound essentially to Sb atoms; only a very weak bonding of O3 with Pb5 was observed. It reflects the relative sta-

bilities of Sb and Pb oxydes and sulfides as a function of $f(O_2)$ and $f(S_2)$ conditions: at increasing $f(O_2)$, stibnite is oxidized before galena. For instance, in the complex sulfide ore of La Bousole deposit (Corbières Massif, France), the coexistence in equilibrium conditions of galena with valentinite, Sb_2O_3, has been observed as a result of partial oxidation of preexisting Pb-Sb sulfosalts (Moëlo, 1983).

Owing to the result of modular analysis of scainiite crystal structure, it is possible to consider new oxygen-enriched shear derivatives of hexagonal parent structures of the zinkenite group by three ways: 1 - substitutions between divalent cations with large ionic radius (Ba, Pb, divalent lanthanides...); 2 - substitutions between trivalent Bi or Sb (perhaps As too); 3- various shear derivatives with increasing oxygen content depending upon the parent structure and the shear amplitude (one-, two-, or even three-octahedra large).

Acknowledgements: We sincerely thank Dr. K. Boubekeur (I.M.N.-L.C.S.) for his help with the Image Plate System. The comments of Drs. E. Makovicky (Geological Institute, Copenhague), Th. Arlt and R.J. Angel (Bayerisches Geoinstitut, Bayreuth) were greatly appreciated. The help of Dr. C. Chopin (E.N.S. Paris) was also greatly appreciated.

References

Aurivillius, B. (1983): The crystal structure of two forms of $BaBi_2S_4$. *Acta Chem. Scand.*, **A37**, 399-407.

Bonazzi, P., Borrini, D., Mazzi, F., Olmi, F. (1995): Crystal structure and twinning of Sb_2AsS_2, the synthetic analogue of pääkkönenite. *Am. Mineral.*, **80**, 1054-1058.

Brese, N. E. & O'Keeffe, M. (1991): Bond-valence parameters for solids. *Acta Cryst.*, **B47**, 192-197.

Gotoh, Y., Akimoto, J., Goto, M., Oosawa, Y., Onoda, M. (1995): The layered composite crystal structure of the ternary sulfide $(BiS)_{1.11}NbS_2$. *J. Solid State Chem.*, **116**, 61-67.

Kupcik, V. (1967): Die Kristallstruktur des Kermesits, Sb_2S_2O. *Sond. Zeit. Naturwiss.*, **5**, S. 114, 1-2.

Lemoine, P., Carré, D., Guittard, M. (1986): Structure du sulfure d'europium et de bismuth $Eu_{1,1}Bi_2S_4$. *Acta Cryst.*, **C42**, 259-261.

Makovicky, E. (1985): Cyclically twinned sulphosalt structures and their approximate analogues. *Z. Kristallogr.*, **173**, 1-23.

— (1989): Modular classification of sulphosalts – current status. Definition and application of homologous series. *N. Jb. Miner. Abh.*, **160**, 269-297.

— (1993): Rod-based sulphosalt structures derived from the SnS and PbS archetypes. *Eur. J. Mineral.*, **5**, 545-591.

Makovicky, E. & Mumme, W.G. (1983): The crystal-structure of ramdohrite, $Pb_6Sb_{11}Ag_3S_{24}$, and its implications for the andorite group and zinckenite. *N. Jb. Miner. Abh.*, **147**, 58-79.

Moëlo, Y. (1979): Quaternary compounds in the system Pb-Sb-S-Cl: dadsonite and synthetic phases. *Can. Mineral.*, **17**, 595-600.

— (1983): Contribution à l'étude des conditions naturelles de formation des sulfures complexes d'antimoine et plomb. B.R.G.M. ed., Orléans, Document **55**, 624 p.

Moëlo, Y., Meerschaut, A., Makovicky, E. (1997): Refinement of the crystal structure of nuffieldite, $Pb_2Cu_{1.4}(Pb_{0.4}Bi_{0.4}Sb_{0.2})Bi_2S_7$: structural relationships and genesis of complex lead sulfosalt structures. *Can. Mineral.*, **35**, 1497-1508.

Orlandi, P., Moëlo, Y., Meerschaut, A., Palvadeau, P. (1999): Lead-antimony sulfosalts from Tuscany (Italy): I – Scainiite, $Pb_{14}Sb_{30}S_{54}O_5$, the first Pb-Sb oxy-sulfosalt, from Buca della Vena mine. *Eur. J. Mineral.*, **11**, 949-954.

Petricek, V., Cisarova, I., de Boer, J.L., Zhou, W., Meetsma, A., Wiegers, G.A., van Smallen, S. (1993): The modulated structure of the commensurate misfit-layer compound $(BiSe)_{1.10}TaSe_2$. *Acta Cryst.*, **B49**, 258-266.

Portheine, J.C. & Nowacki, W. (1975): Refinement of the crystal structure of zinckenite, $Pb_6Sb_{14}S_{27}$. *Z. Kristallogr.*, **141**, 79-96.

Ren, Y., Meetsma, A., Petricek, V., van Smaalen, S., Wiegers, G.A. (1995): (3 + 2)-dimensional superspace approach to the structure of the incommensurate intergrowth compound: $(SbS)_{1.15}TiS_2$. *Acta Cryst.*, **B51**, 275-287.

Ren, Y., Meetsma, A., Wiegers, G.A., van Smaalen, S. (1996): (3 + 2)-dimensional superspace approach to the structure of the stage-2 misfit layer compound: $(SbS)_{1.15}(TiS_2)_2$. *Acta Cryst.*, **B52**, 389-397.

Sheldrick, G.M. (1996): SHELXTL Version 5. An integrated system for solving, refining and displaying crystal structures from diffraction data. Siemens Analytical X-ray Instruments Inc., Madison, Wisconsin (U.S.A.).

Stoe (1996): Imaging Plate Diffractometer System, version 2.75. Stoe & Cie edit., Darmstadt (Germany).

Sutorik, A. & Kanatzidis, M.G. (1994): $Ba_6Ti_5S_{15}O$: A new metal/oxysulfide resulting from the inclusion of BaO into the $BaTiS_3$ structure type. *Chem. Mater.*, **6**, 1700-1704.

Zhou, W.Y., Meetsma, A., de Boer, J.L., Wiegers, G.A. (1992): Characterization and electrical transport properties of the misfit layer compounds $(BiSe)_{1.10}NbSe_2$ and $(BiSe)_{1.10}TaSe_2$. *Mat. Res. Bull.*, **27**, 563-572.

Received 11 March 1999
Modified version received 8 November 1999
Accepted 9 February 2000

Erratum: In the abstract of the definition of scainiite (Orlandi *et al.*, 1999), one index (6 2 4) of the X-ray diffraction line at 2.956 Å must be replaced by the index $(\bar{1}2\ 2\ 2)$ (see Table 2).